

JD9: Cold Gas and Dust at High Redshift
Highlights of Astronomy, Vol. 12, 2000
D.J. Wilner, ed.

TYPE 1 AGN AND THEIR LINK TO ULIRGS

Paola Andreani

Osservatorio Astronomico di Padova, Padova, Italy

Max-Planck Institut f. Extraterrestrische Physik, Garching, Germany

e-mail: andreani@pd.astro.it

Abstract. Increasing observational evidence supports a picture for a close link among AGN phenomenon, star-formation processes and galaxy formation. Since the physical phenomena related to the onset of both AGN and star formation are very likely characterized by a strong far infrared (FIR) emission it becomes mandatory to investigate the FIR energy domain. However, because of their faintness in the FIR energy range, very little is known about the FIR properties of type 1 AGN, and type 2 AGN, which are supposed to be missed in classical searches, still lack definition and samples.

Our aim is to investigate the FIR properties of optically selected type 1 AGN, compare them to Ultraluminous Infrared Galaxies (ULIRGs) and derive some general characteristics of the population. Expectations for future surveys are also presented.

1. Introduction

For historical reasons and selection criteria, a classical type 1 AGN is that showing a spectral energy distribution (SED) with most of its energy in the UV and only 10 - 20 % in the infrared. From $10\text{ }\mu\text{m}$ to $1000\text{ }\text{\AA}$ the agreement among different composite spectra, built on observations from different databases, is excellent, while in the FIR the various studies disagree. The FIR SED differs not only in shape but also the FIR luminosity differs by up two order of magnitudes. This difference is due to inhomogeneities of AGN samples, covering different luminosity ranges and objects selected according to different criteria. However a common result of these studies is that both AGN and starburst (SB) dominated objects have a common FIR-emitting star-formation component from which is not easy to disentangle pure AGN emission. Quite a number of observational evidence supports the above claim: (a) their $60\text{ }\mu\text{m}$ flux, radio and CO emissions are well correlated and AGN and star-forming galaxies show the same properties; (b) their SEDs at $\lambda > 60\text{ }\mu\text{m}$ have the same shape as those of star-forming regions; (c) the FIR Luminosity Function of AGN coincides with that of SBs in shape and differ only in amplitude: $\Phi_{AGN}^*/\Phi_{SB}^* = 1/25$; (d) the evolution rate of the two classes is comparable and shows the same behaviour $L(z) \propto (1+z)^{2\div 3}$ (e) the FIR component represents a distinct component correlating only weakly with the true AGN emission and very likely related to a concurrent SB (Lawrence, 2001; Rowan-Robinson, 2001).

All this supports the idea that all AGN are accompanied by a SB but one SB out of 25 is accompanied by an AGN. There are indeed evidences for a coexistence of central AGN and circumnuclear star formation in a significant fraction of ULIRGs (Genzel et al., 1998) but AGN are difficult to be observationally proved mainly because of the high extinction of the nuclear source. Other distinct direct and indirect observational probes indicate that an unknown fraction of AGN is absorbed, the so-called type 2, and the ratio between type 2 and type 1 may be as high as 10 of which 20 percent in FIR selected objects. For instance, the comoving mass density of Massive Dark Objects, which are probably supermassive Black Holes in galaxy centers, are a factor of 2 or larger than that explained by accretion onto optically-luminous AGN. This implies that much accretion is obscured by dust (Haehnelt, Natarajan and Rees, 1998) a population which is missing in optically selected samples. Other evidences come from X-ray studies and are extensively discussed in this volume.

Dust enshrouded type 1 AGN exist at high and low redshifts and constitute a subset of SCUBA galaxies, which in turn share common properties with local ULIRGs. Nearly all nearby ULIRGs appear to be late-stage mergers, then if one out 10 SB has quasar-like activity is then possible to envisage the evolutionary path starting from a merging system going through a starburst and ending to a optical-phase QSO (Sanders et al., 1989).

2. Present work

The aim of the present work is to use FIR observations, gathered by the Infrared Space Observatory (ISO), of optical AGN to infer any evolutionary link from ‘pure’ AGN objects to eventual transition objects linking AGN to ULIRGs.

This aim was pursued by comparing FIR and optical properties in a complete subsample of optically selected bright ($15 \leq B \leq 17$) quasars. The sample completeness ensures a better control of observational biases and provides reliable information on the properties of the underlying population. The objects studied in this work can be then fully considered as representative of the entire population. The optical observations consist of multicolour (U,B,V,R,I) broadband photometry used primarily to selected quasars candidates, which were then later spectroscopically confirmed. ISO FIR photometry has been taken at 7,12,25,60,100 and 160 μm . All the details of these observations and the sample properties can be found in Andreani et al. (2001).

3. A colour-colour diagramme for QSOs

Figure 1(A) reports $\alpha(60\mu\text{m}, \text{MIR})$ versus $\alpha(\text{FIR}, 60\mu\text{m})$. By MIR we indicate the mid-IR bands 7, 12 and 25 μm and by FIR the far-IR bands at 100 and 160 μm . α are the spectral indices, i.e. for a $f_\nu \propto \nu^\alpha$ SED: $\alpha(\nu_1, \nu_2) = \log(f(\nu_1)/f(\nu_2)) - \log(\nu_1/\nu_2)$ and are therefore simply related to colours. Our results (see Andreani et al., 2001) indicate that $\alpha(\text{FIR}, 60\mu\text{m})$ is a fair estimate of T_{wd}^{-1} , where T_{wd} is the temperature of a **warm** dust component.

The diagram shows a trend: the relative emission at MIR (shorter) wavelengths

with respect to the $60\mu\text{m}$ emission decreases as T_{wd} increases. A possible interpretation is the increasing dominance of SB component with respect to AGN in objects with lower values of T_{wd} and lower values of the ratio $F(60\mu\text{m})/F(\text{MIR})$. The colour-colour diagram was indeed widely used in the past as a tool to detect and discriminate between different types of activity in the nuclear and circum-nuclear regions of galaxies (see e.g., Canalizo & Stockton (2001) and references therein). Different kind of objects (QSOs/Seyferts, starbursts and ULIRGS) occupy distinct areas of such a diagram: where FIR fluxes are dominated by dust reradiation objects locate in the lower right corner (in our convention at lower T_{wd} and lower $\alpha(60\mu\text{m}, \text{MIR})$) while those with strong non-thermal emission, such as optically selected QSOs, are in the upper left corner. This means that our sample spans a wide range of properties from those ‘AGN pure’ to those where a concurrent SB dominates.

4. The type 1 SED

By making the rather coarse assumption that optical quasars can thus be modeled as a homogeneous population, observations at fixed frequencies of targets at different redshifts can be then used to build the entire SED for this population. This analysis exploits the whole spectral information from the optical to the FIR and helps outlining possible general features of the emitting mechanisms and the physics of the QSO environment.

The spectrum is built by dividing the available wavelength range in bins. In each bin an average of the fluxes at that wavelength is computed. The errorbars shown are those related to the averages but take into account also photometric uncertainties. Figure 1(B) reports the average spectrum in the QSO restframe. A well defined IR component peaking at $10\text{-}30\ \mu\text{m}$ and dropping steeply above $100\ \mu\text{m}$ is evident. Although from the characteristic shape it is quite straightforward to infer a thermal origin for this component it can be due either to a SB emission in the host galaxy and/or to a dusty torus around the central source. When comparing these data with models (Granato & Danese, 1994) it is possible to bound the available parameters on the dust distribution. It turns out that the dust distribution around the central source should be compact because of the sharp cut-off at long wavelengths of the FIR bump. A larger bump would imply larger temperature distribution and very likely larger spatial dimension of the dust distribution. Furthermore, the data are better in agreement with models predicting the strongest dust self-absorption around $10\text{-}30\ \mu\text{m}$.

5. Expected counts of Type 1 AGN

Based on these results we show here the predictions of simple models on the expected numbers of type 1 QSOs in deep future surveys such those foreseen with SIRT-F and HERSCHEL Satellites.

As well known number counts of extragalactic objects represent one of the fundamental tool to investigate galaxy evolution, since they are related to the Luminosity Function. The differential counts, $dN(S)/dS$, can be expressed as a

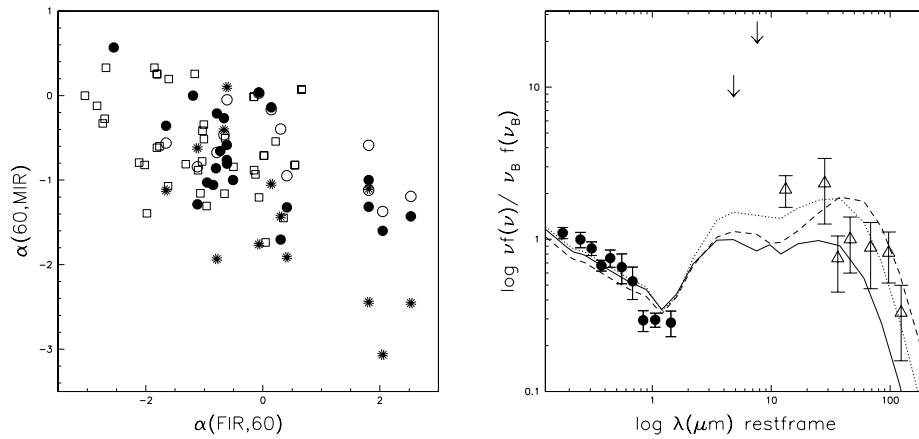


Figure 1. Left (A): The ratio between $60\mu\text{m}$ flux and MIR fluxes is shown as a function of the ratio between FIR and $60\mu\text{m}$ fluxes. Asterisks correspond to the $25\mu\text{m}$ data, filled squares to $12\mu\text{m}$, open circles to $7\mu\text{m}$ ones. Open squares correspond to QSOs at $z \leq 2$ reported in Andreani, Franceschini & Granato (1999). Distinct areas can be identified from AGN dominated (in the upper left corner) to SB dominated objects (in the lower right corner), according to the expected dominant emitting mechanism in the object SED from non-thermal to thermal. Right (B): The average spectrum in the QSO restframe. The spectrum is normalized at $\lambda_{\text{blue}} = 0.44\mu\text{m}$. Filled circles correspond to the optical and near-IR data, open triangles to the ISO measurements. The lines going through the data show the predictions of models by Granato and Danese (1994). The solid line corresponds to a face-on compact configuration of the torus with absorption at $30\mu\text{m}$ of $\tau=30$; the dotted and dashed lines to a 45° inclined torus with larger dimension and $\tau=30$ and $\tau=60$, respectively.

simple integral of the epoch-dependent luminosity function, $\Psi(L, z)$:

$$\frac{dN}{dS} = \int_{z_l}^{z_u} dz \frac{dV}{dz} \frac{dL(S, z)}{dS} \Psi[L(S, z), z] \quad \text{sources/sr} \quad (1)$$

where z_u and z_l being the effective upper and lower limits of the redshift distribution and $\frac{dV}{dz}$ the differential comoving volume. The integrated counts are easily found by integrating eq.(1) at different flux limits, S .

As $\Psi(L, z)$ we take the B-band luminosity function that computed by Boyle et al. (2001) and as its redshift evolution that described in Bianchi, Cristiani & Tae-Sum (2001). The latter has a down-turn at $z = 3$ and decays exponentially until $z = 10$. The cosmological parameters used to compute the differential volume are $H_0 = 50$ km/s/Mpc, $\Omega = 1$, $\Lambda = 0$. We compute k-corrections, i.e. $dL(S, z)/dS$, according to the composite spectrum of Figure 1(B) and plot in Figure 2 the expected counts in different observing bands: 5, 8, 24 and $60\mu\text{m}$. i.e. those corresponding to the filter sets of IRAC and MIPS on board of SIRT-F and PACS on board of Herschel. It is easily shown that for a deep survey in a sky area of 0.3deg^2 at a depth of 0.4 mJy at $24\mu\text{m}$ and of $34\mu\text{Jy}$ at $8\mu\text{m}$ we expect to see with SIRT-F a few tens and a few hundreds objects, respectively. Note that the numbers presented here refer to an ideal survey not affected by observational uncertainties (confusion noise, photometric errors, ...). More realistic predictions taking into account also the selection of candidate QSOs will be the subject of a forthcoming paper.

Table 1. Expected counts of type-1 AGN in future IR surveys

λ (μm)	S_{\min} (μJy)	sky area (deg^2)	# of objects	Instrument
4.5	5	0.3	1000	IRAC/SIRT-F
8.0	34	0.3	350	IRAC/SIRT-F
24	370	0.3	50	MIPS/SIRT-F
75	5000	1.0	22	PACS/HSO

References

Andreani P., Franceschini A., Granato G.L., 1999 MNRAS 306, 161
 Andreani P. et al., 2001, A&A, submitted
 Bianchi S., Cristiani S., Tae-Sum K., 2001, A&A, in press
 Boyle B.J. et al., 2001, MNRAS 317, 1014
 Canalizo G., Stockton A., 2001, ApJ 555, 719
 Genzel R. et al., 1998, ApJ 498, 579
 Granato G.L., Danese L., 1994, MNRAS 268, 235
 Haehnelt M.G., Natarajan P. & Rees M.J., 1998, MNRAS 303, 179
 Lawrence A., 2001, in the *Promise of FIRST*, ESA Symposium, Dec. 12-15 2000
 Toledo Spain, eds Pilbratt G.L. et al.
 Rowan-Robinson M., 2001, ApJ 549, 745
 Sanders D.B. et al., 1989, ApJ 347, 29

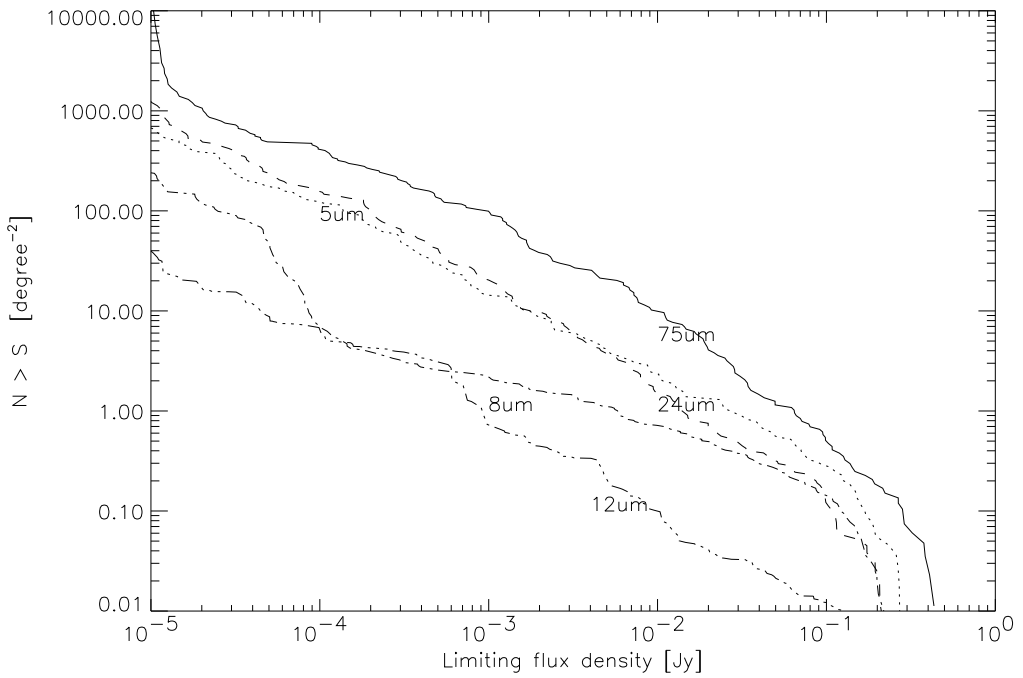


Figure 2. Expected number counts of type 1 AGN computed on the basis of the composite SED of the type 1 AGN of the sample presented in this work. The different wavelengths correspond to the bands of IRAC and MIPS instruments on board of SIRT-F and PACS on board of Herschel. 12 μ m counts are only shown for comparison.